**The Abdus Salam**
**International Centre for Theoretical Physics**
**Strada Costiera, 11 I - 34151 Trieste, Italy**
**Earth System Physics Section - ESP**

# Regional Climatic Model RegCM User Manual
# Version 4.3

Nellie Elguindi, Xunqiang Bi, Filippo Giorgi,
Badrinath Nagarajan, Jeremy Pal, Fabien Solmon,
Sara Rauscher, Ashraf Zakey, Travis O'Brien,
and Graziano Giuliani
Trieste, Italy
January 2013

## Acknowledgements

This paper is dedicated to those that have contributed to the growth of RegCM system over the past 20+ years, the members (800+) of the RegCNET, and the ICTP.

# Contents


**1 The REGional Climate Model (RegCM) 9**

**2 Description 10**
2.1 History . . . 10
2.2 Model components . . . 11
2.3 The RegCM Model Horizontal and Vertical Grid . . . 12
2.4 Map Projections and Map-Scale Factors . . . 13

**3 Model Physics 15**
3.1 Dynamics . . . 15
3.1.1 Horizontal Momentum Equations . . . 15
3.1.2 Continuity and Sigmadot ($\dot{\sigma}$) Equations . . . 15
3.1.3 Thermodynamic Equation and Equation for Omega ($\omega$) . . . 16
3.1.4 Hydrostatic Equation . . . 16
3.2 Physics parametrizations . . . 17
3.2.1 Radiation Scheme . . . 17
3.2.2 Land Surface Models . . . 17
3.2.3 Planetary Boundary Layer Scheme . . . 20
3.2.4 Convective Precipitation Schemes . . . 22
3.2.5 Large-Scale Precipitation Scheme . . . 24
3.2.6 Ocean flux Parameterization . . . 25
3.2.7 Prognostic Sea Surface Skin Temperature Scheme . . . 26
3.2.8 Pressure Gradient Scheme . . . 26
3.2.9 Lake Model . . . 26
3.2.10 Aerosols and Dust (Chemistry Model) . . . 27

**4 Future Developments 28**
4.1 Tiedtke convection scheme . . . 28
4.2 Semi-Lagrangian dynamic core . . . 28
4.3 Non-Hydrostatic core . . . 28

# List of Figures

2.1 Schematic representation of the vertical structure of the model. This example is for 16 vertical layers. Dashed lines denote half-sigma levels, solid lines denote full-sigma levels. (Adapted from the PSU/NCAR Mesoscale Modeling System Tutorial Class Notes and User's Guide.) . . . . . 12
2.2 Schematic representation showing the horizontal Arakawa B-grid staggering of the dot and cross grid points. . . . . 13

# List of Tables

3.1 Land Cover/Vegetation classes . . . . . 18
3.2 BATS vegetation/land-cover . . . . . 19
3.3 Resolution for CLM input parameters . . . . . 20

# Chapter 1

# The RegCM

The RegCM is a regional climate model developed throughout the years, with a wide base of model users. It has evolved from the first version developed in the late eighties (RegCM1, *Dickinson et al.* [1989]), *Giorgi* [1990]), to later versions in the early nineties (RegCM2, *Giorgi et al.* [1993b], *Giorgi et al.* [1993c]), late nineties (RegCM2.5, *Giorgi and Mearns* [1999]) and 2000s (RegCM3, *Pal et al.* [2000]).

The RegCM has been the first limited area model developed for long term regional climate simulation, it has participated to numerous regional model intercomparison projects, and it has been applied by a large community for a wide range of regional climate studies, from process studies to paleo-climate and future climate projections (*Giorgi and Mearns* [1999], *Giorgi et al.* [2006]).

The RegCM system is a community model, and in particular it is designed for use by a varied community composed by scientists in industrialized countries as well as developing nations (*Pal et al.* [2007]).

As such, it is designed to be a public, open source, user friendly and portable code that can be applied to any region of the World. It is supported through the Regional Climate research NETwork, or RegCNET, a widespread network of scientists coordinated by the Earth System Physics section of the Abdus Salam International Centre for Theoretical Physics Abdus Salam International Centre for Theoretical Physics (ICTP), being the foster the growth of advanced studies and research in developing countries one of the main aims of the ICTP.

The home of the model is:

**http://users.ictp.it/RegCNET**

Scientists across this network (currently subscribed by over 750 participants) can communicate through an email list and via regular scientific workshops, and they have been essential for the evaluation and sequential improvements of the model.

Since the release of RegCM3 described by *Pal et al.* [2007], the model has undergone a substantial evolution both in terms of software code and physics representations, and this has lead to the development of a fourth version of the model, RegCM4, which was released by the ICTP in June 2010 as a prototype version (RegCM4.0) and in May 2011 as a first complete version (RegCM4.1).

The purpose of this Manual is to provide a basic reference for RegCM4, with a description of the model, with a special accent to the improvements recently introduced. Compared to previous versions, RegCM4 includes new land surface, planetary boundary layer and air-sea flux schemes, a mixed convection and tropical band configuration, modifications to the pre-existing radiative transfer and boundary layer schemes and a full upgrade of the model code towards improved flexibility, portability and user friendliness.

The model can be interactively coupled to a 1D lake model, a simplified aerosol scheme (including OC, BC, SO4, dust and sea spray) and a gas phase chemistry module (CBM-Z). Overall, RegCM4 shows an improved performance in several respects compared to previous versions, although further testing by the user community is needed to fully explore its sensitivities and range of applications.

The RegCM is available on the World Wide Web thanks to the Democritos Italy CNR group at:

**https://eforge.escience-lab.org/gf/project/regcm**

# Chapter 2

# Description

## 2.1 History

The idea that limited area models (LAMs) could be used for regional studies was originally proposed by *Dickinson et al.* [1989] and *Giorgi* [1990].

This idea was based on the concept of one-way nesting, in which large scale meteorological fields from General Circulation Model (GCM) runs provide initial and time-dependent meteorological lateral boundary conditions (LBCs) for high resolution Regional Climate Model (RCM) simulations, with no feedback from the RCM to the driving GCM.

The first generation NCAR RegCM was built upon the National Center for Atmospheric Research (NCAR)-Pennsylvania State University (PSU) Mesoscale Model version 4 (MM4) in the late 1980s [*Dickinson et al.*, 1989; *Giorgi*, 1989]. The dynamical component of the model originated from the MM4, which is a compressible, finite difference model with hydrostatic balance and vertical $\sigma$-coordinates.

Later, the use of a split-explicit time integration scheme was added along with an algorithm for reducing horizontal diffusion in the presence of steep topographical gradients [*Giorgi et al.*, 1993a, b].

As a result, the dynamical core of the RegCM is similar to that of the hydrostatic version of Mesoscale Model version 5 (MM5) [*Grell et al.*, 1994]: the RegCM4 is thus a hydrostatic, compressible, sigma-p vertical coordinate model run on an Arakawa B-grid in which wind and thermodynamical variables are horizontally staggered using a time-splitting explicit integration scheme in which the two fastest gravity modes are first separated from the model solution and then integrated with smaller time steps.

For application of the MM4 to climate studies, a number of physics parameterizations were replaced, mostly in the areas of radiative transfer and land surface physics, which led to the first generation RegCM [*Dickinson et al.*, 1989; *Giorgi*, 1990]. The first generation RegCM included the Biosphere-Atmosphere Transfer Scheme, BATS, [*Dickinson et al.*, 1986] for surface process representation, the radiative transfer scheme of the Community Climate Model version 1 (CCM1), a medium resolution local planetary boundary layer scheme, the Kuo-type cumulus convection scheme of [*Anthes*, 1977] and the explicit moisture scheme of [*Hsie et al.*, 1984].

A first major upgrade of the model physics and numerical schemes was documented by [*Giorgi et al.*, 1993a, b], and resulted in a second generation RegCM, hereafter referred to as REGional Climate Model version 2 (RegCM2). The physics of RegCM2 was based on that of the NCAR Community Climate Model version 2 (CCM2) [*Hack et al.*, 1993], and the mesoscale model MM5 [*Grell et al.*, 1994]. In particular, the CCM2 radiative transfer package [*Briegleb*, 1992] was used for radiation calculations, the non local boundary layer scheme of [*Holtslag et al.*, 1990] replaced the older local scheme, the mass flux cumulus cloud scheme of [*Grell*, 1993] was added as an option, and the latest version of BATS1E [*Dickinson et al.*, 1993] was included in the model.

In the last few years, some new physics schemes have become available for use in the RegCM, mostly based on physics schemes of the latest version of the Community Climate Model (CCM), Community Climate Model version 3 (CCM3) [*Kiehl et al.*, 1996]. First, the CCM2 radiative transfer package has been replaced by that of the CCM3. In the CCM2 package, the effects of $H_2O$, $O_3$, $O_2$, $CO_2$ and clouds were accounted for by the model. Solar radiative transfer was treated with a $\delta$-Eddington approach and cloud radiation depended on three cloud parameters, the cloud fractional cover, the cloud liquid water content, and the cloud effective droplet radius. The CCM3 scheme retains the same structure as that of the CCM2, but it includes new features such as the effect of additional greenhouse gases ($NO_2, CH_4$, CFCs), atmospheric aerosols, and cloud ice. Scattering and absorption of

solar radiation by aerosols are also included based on the aerosol optical properties (Absorption Coefficient and Single Scattering Albedo).

A simplified explicit moisture scheme *Hsie et al.* [1984] is included, where only a prognostic equation for cloud water is used, which accounts for cloud water formation, advection and mixing by turbulence, re-evaporation in sub-saturated conditions, and conversion into rain via a bulk autoconversion term. Prognosed cloud water variable is directly used in the cloud radiation calculations, and not diagnosed in terms of the local relative humidity, adding a very important and far reaching element of interaction between the simulated hydrologic cycle and energy budget calculations.

The solar spectrum optical properties are based on the cloud liquid water path, which is in turn based on the cloud liquid water amount prognostically calculated by the model, cloud fractional cover, which is calculated diagnostically as a function of relative humidity, and effective cloud droplet radius, which is parameterized as a function of temperature and land sea mask for liquid water and as a function of height for ice phase.

In addition, the scheme diagnostically calculates a fraction of cloud ice as a function of temperature. In the infrared spectrum the cloud emissivity is calculated as a function of cloud liquid/ice water path and cloud infrared absorption cross sections depending on effective radii for the liquid and ice phase.

One of the problems in this formulation is that the scheme uses the cloud fractional cover to produce grid box mean cloud properties which are then treated as if the entire grid box was covered by an effectively thinner cloud layer. However, because of the non-linear nature of radiative transfer, this approach tends to produce a grayer mean grid box than if separate cloudy and clear sky fractional fluxes were calculated. By taking advantage of the fact that the scheme also calculates clear sky fluxes for diagnostic purposes, in iRegCM4 we modified this radiative cloud representation by first calculating the total cloud cover at a given grid point and then calculating the surface fluxes separately for the cloudy and clear sky portions of the grid box.

The total cloud cover at a model grid box is given by a value intermediate between that obtained using the random overlap assumption (which maximizes cloud cover) and that given by the largest cloud cover found in any single layer of the column overlying the grid box (which implies a full overlap and it is thus is a minimum estimate of total cloud cover).

This modification thus accounts for the occurrence of fractional clear sky at a given grid box, leading to more realistic grid-box average surface radiative fluxes in fractional cloudy conditions.

A large-scale cloud and precipitation scheme which accounts for the subgrid-scale variability of clouds [*Pal et al.*, 2000], parameterizations for ocean surface fluxes [*Zeng et al.*, 1998], and multiple cumulus convection scheme [*Anthes*, 1977; *Grell*, 1993; *Emanuel*, 1991; *Emanuel and Zivkovic-Rothman*, 1999] are the same as in RegCM3, but a new ”mixed scheme” Grell+Emanuel is introduced: it allows the user to select one of the two schemes in function of the ocean-land mask.

The other main development compared to RegCM3 concerns the aerosol radiative transfer calculations. In RegCM3 the aerosol radiative forcing was based on three dimensional fields produced by the aerosol model, and included only scattering and absorption in the shortwave spectrum (see *Giorgi et al.* [2002]). In RegCM4 we added the contribution of the infrared spectrum following *Solmon et al.* [2008].

This is especially important for relatively large dust and sea salt particles and it is calculated by introducing an aerosol infrared emissivity calculated as a function of aerosol path and absorption cross section estimated from aerosol size distribution and long wave refractive indices. Long wave diffusion, which could be relevant for larger dust particles, is not treated as part of this scheme.

The mosaic-type parameterization of subgrid-scale heterogeneity in topography and land use [*Giorgi et al.*, 2003b] allows finer surface resolution in the Biosphere-Atmosphere Transfer Scheme version 1e (BATS1e).

## 2.2 Model components

The RegCM modeling system has four components: Terrain, ICBC, RegCM, and Postprocessor. Terrain and ICBC are the two components of RegCM preprocessor. Terrestrial variables (including elevation, landuse and sea surface temperature) and three-dimensional isobaric meteorological data are horizontally interpolated from a latitude-longitude mesh to a high-resolution domain on either a Rotated (and Normal) Mercator, Lambert Conformal, or Polar Stereographic projection. Vertical interpolation from pressure levels to the $\sigma$ coordinate system of RegCM is also performed. $\sigma$ surfaces near the ground closely follow the terrain, and the higher-level $\sigma$ surfaces tend to approximate isobaric surfaces.

Since the vertical and horizontal resolution and domain size can vary, the modeling package programs employ

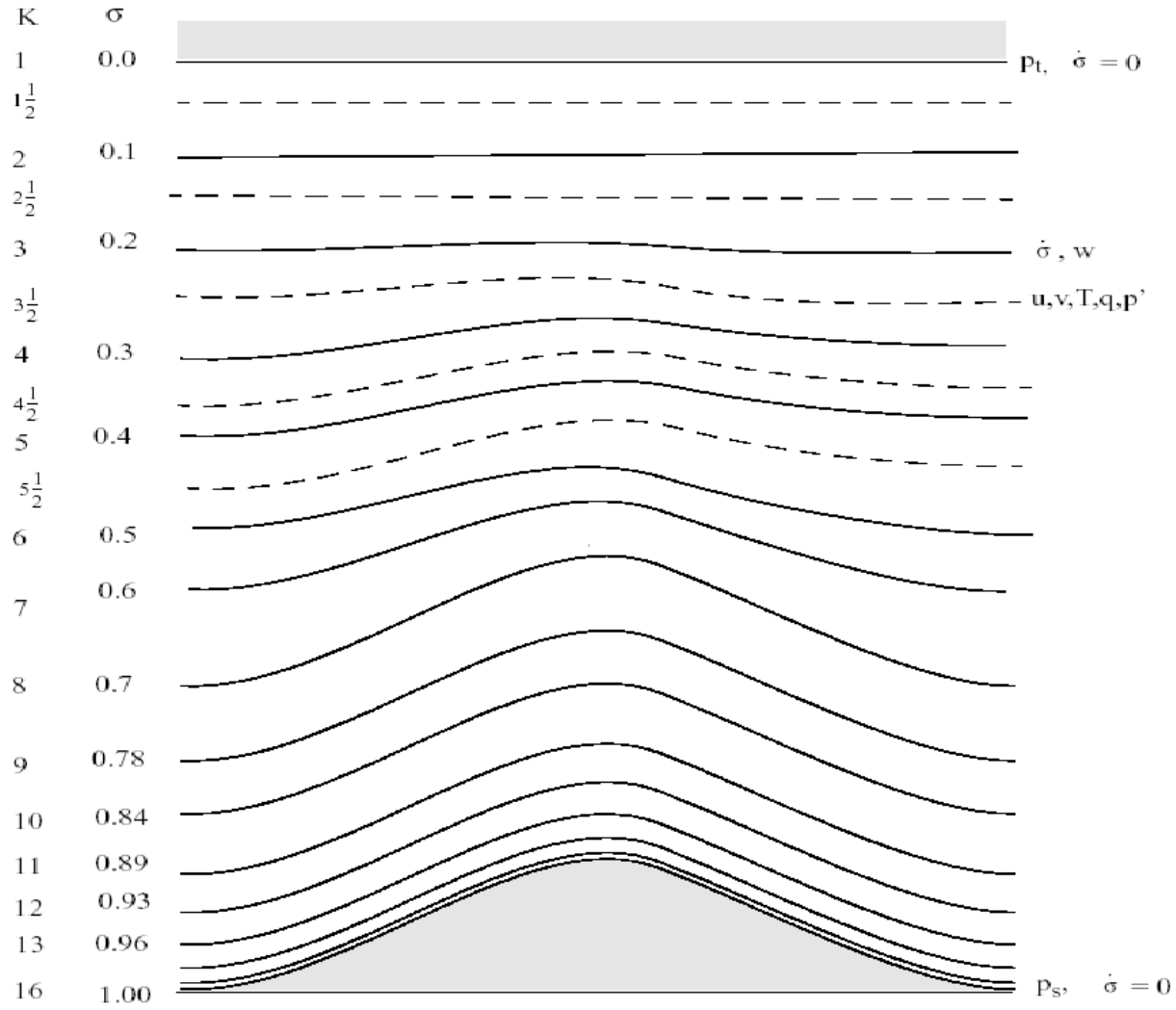


Figure 2.1: Schematic representation of the vertical structure of the model. This example is for 16 vertical layers. Dashed lines denote half-sigma levels, solid lines denote full-sigma levels. (Adapted from the PSU/NCAR Mesoscale Modeling System Tutorial Class Notes and User's Guide.)

parameterized dimensions requiring a variable amount of core memory, and the requisite hard-disk storage amount is varied accordingly.

## 2.3 The RegCM Model Horizontal and Vertical Grid

It is useful to first introduce the model's grid configuration. The modeling system usually gets and analyzes its data on pressure surfaces, but these have to be interpolated to the model's vertical coordinate before input to the model. The vertical coordinate is terrain-following (Figure 2.1) meaning that the lower grid levels follow the terrain while the upper surface is flatter. Intermediate levels progressively flatten as the pressure decreases toward the top of the model. A dimensionless $\sigma$ coordinate is used to define the model levels where $p$ is the pressure, $p_t$ is a specified constant top pressure, $p_s$ is the surface pressure.

$$\sigma = \frac{(p - p_t)}{(p_s - p_t)} \tag{2.1}$$

It can be seen from the equation and Figure 2.1 that $\sigma$ is zero at the top and one at the surface, and each model level is defined by a value of $\sigma$. The model vertical resolution is defined by a list of values between zero and one

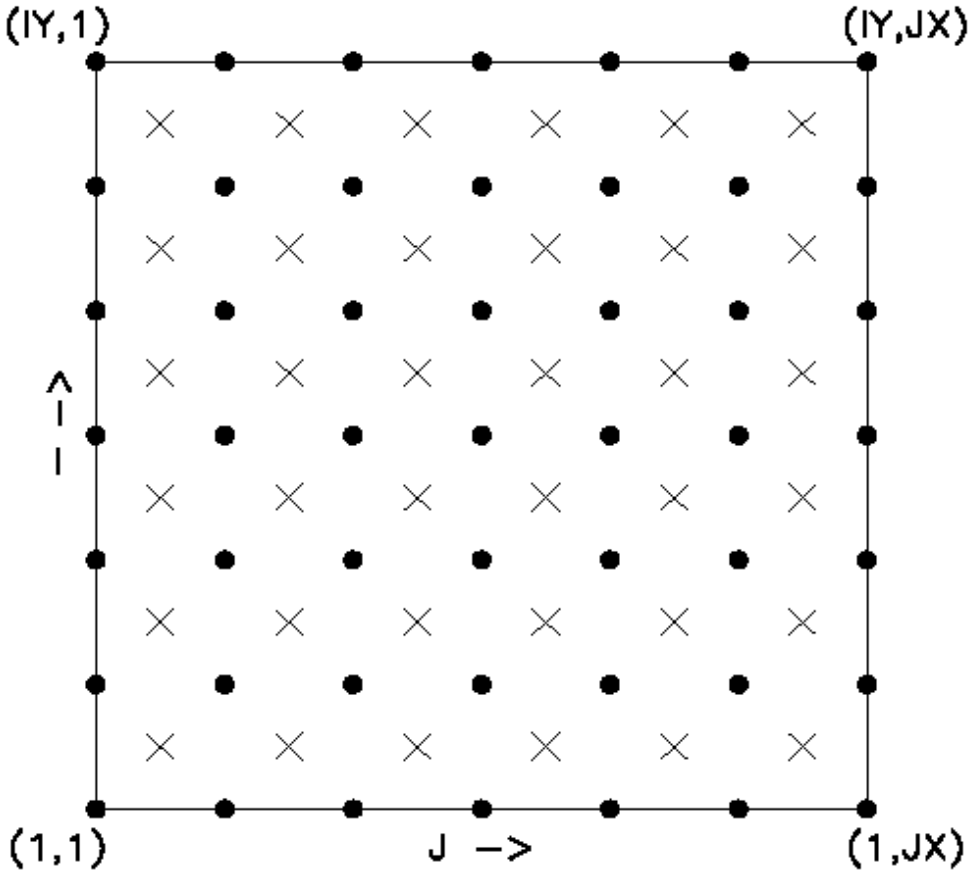


Figure 2.2: Schematic representation showing the horizontal Arakawa B-grid staggering of the dot and cross grid points.

that do not necessarily have to be evenly spaced. Commonly the resolution in the boundary layer is much finer than above, and the number of levels may vary upon the user demand.

The horizontal grid has an Arakawa-Lamb B-staggering of the velocity variables with respect to the scalar variables. This is shown in Figure 2.2 where it can be seen that the scalars (T, q, p, etc) are defined at the center of the grid box, while the eastward (u) and northward (v) velocity components are collocated at the corners. The center points of grid squares will be referred to as cross points, and the corner points are dot points. Hence horizontal velocity is defined at dot points. Data is input to the model, the preprocessors do the necessary interpolation to assure consistency with the grid.

All the above variables are defined in the middle of each model vertical layer, referred to as half-levels and represented by the dashed lines in Figure 2.1. Vertical velocity is carried at the full levels (solid lines). In defining the sigma levels it is the full levels that are listed, including levels at $\sigma = 0$ and 1. The number of model layers is therefore always one less than the number of full sigma levels.

The finite differencing in the model is, of course, crucially dependent upon the grid staggering wherever gradients or averaging are represented terms in the equation.

## 2.4 Map Projections and Map-Scale Factors

The modeling system has a choice of four map projections. Lambert Conformal is suitable for mid-latitudes, Polar Stereographic for high latitudes, Normal Mercator for low latitudes, and Rotated Mercator for extra choice. The

*x* and *y* directions in the model do not correspond to west-east and north-south except for the Normal Mercator projection, and therefore the observed wind generally has to be rotated to the model grid, and the model *u* and *v* components need to be rotated before comparison with observations. These transformations are accounted for in the model pre-processors that provide data on the model grid (Please note that model output of u and v components, raw or postprocessed, should be rotated to a lat/lon grid before comparing to observations). The map scale factor, *m*, is defined by

*m* = (distance on grid) / (actual distance on earth)

and its value is usually close to one, varying with latitude. The projections in the model preserve the shape of small areas, so that dx=dy everywhere, but the grid length varies across the domain to allow a representation of a spherical surface on a plane surface. Map-scale factors need to be accounted for in the model equations wherever horizontal gradients are used.

# Chapter 3

# Model Physics

## 3.1 Dynamics

The model dynamic equations and numerical discretization are described by *Grell et al.* [1994].

### 3.1.1 Horizontal Momentum Equations

$$\frac{\partial p^* u}{\partial t} = -m^2 \left( \frac{\partial p^* uu/m}{\partial x} + \frac{\partial p^* vu/m}{\partial y} \right) - \frac{\partial p^* u\dot{\sigma}}{\partial \sigma} - mp^* \left[ \frac{RT_v}{(p^* + p_t/\sigma)} \frac{\partial p^*}{\partial x} + \frac{\partial \phi}{\partial x} \right] + f p^* v + F_H u + F_V u, \tag{3.1}$$

$$\frac{\partial p^* v}{\partial t} = -m^2 \left( \frac{\partial p^* uv/m}{\partial x} + \frac{\partial p^* vv/m}{\partial y} \right) - \frac{\partial p^* v\dot{\sigma}}{\partial \sigma} - mp^* \left[ \frac{RT_v}{(p^* + p_t/\sigma)} \frac{\partial p^*}{\partial y} + \frac{\partial \phi}{\partial y} \right] + f p^* u + F_H v + F_V v, \tag{3.2}$$

where $u$ and $v$ are the eastward and northward components of velocity, $T_v$ is virtual temperature, $\phi$ is geopotential height, $f$ is the coriolis parameter, $R$ is the gas constant for dry air, $m$ is the map scale factor for either the Polar Stereographic, Lambert Conformal, or Mercator map projections, $\dot{\sigma} = \frac{d\sigma}{dt}$, and $F_H$ and $F_V$ represent the effects of horizontal and vertical diffusion, and $p^* = p_s - p_t$.

### 3.1.2 Continuity and Sigmadot $(\dot{\sigma})$ Equations

$$\frac{\partial p^*}{\partial t} = -m^2 \left( \frac{\partial p^* u/m}{\partial x} + \frac{\partial p^* v/m}{\partial y} \right) - \frac{\partial p^* \dot{\sigma}}{\partial \sigma}. \tag{3.3}$$

The vertical integral of Equation 3.3 is used to compute the temporal variation of the surface pressure in the model,

$$\frac{\partial p^*}{\partial t} = -m^2 \int_0^1 \left( \frac{\partial p^* u/m}{\partial x} + \frac{\partial p^* v/m}{\partial y} \right) d\sigma. \tag{3.4}$$

After calculation of the surface-pressure tendency $\frac{\partial p^*}{\partial t}$, the vertical velocity in sigma coordinates $(\dot{\sigma})$ is computed at each level in the model from the vertical integral of Equation 3.3.

$$\dot{\sigma} = -\frac{1}{p^*}\int_0^{\sigma}\left[\frac{\partial p^*}{\partial t} + m^2\left(\frac{\partial p^* u/m}{\partial x} + \frac{\partial p^* v/m}{\partial y}\right)\right] d\sigma\prime \tag{3.5}$$

where $\sigma\prime$ is a dummy variable of integration and $\dot{\sigma}(\sigma = 0) = 0$.

### 3.1.3 Thermodynamic Equation and Equation for Omega $(\omega)$

The thermodynamic equation is

$$\frac{\partial p^* T}{\partial t} = -m^2\left(\frac{\partial p^* uT/m}{\partial x} + \frac{\partial p^* vT/m}{\partial y}\right) - \frac{\partial p^* T\dot{\sigma}}{\partial \sigma} + \frac{RT_v\omega}{c_{pm}(\sigma + P_t/p_{ast})} + \frac{p^* Q}{c_{pm}} + F_H T + F_V T \tag{3.6}$$

where $c_{pm}$ is the specific heat for moist air at constant pressure, $Q$ is the diabatic heating, $F_H T$ represents the effect of horizontal diffusion, $F_V T$ represents the effect of vertical mixing and dry convective adjustment, and $\omega$ is

$$\omega = p^*\dot{\sigma} + \sigma\frac{dp^*}{dt} \tag{3.7}$$

where,

$$\frac{dp^*}{dt} = \frac{\partial p^*}{\partial t} + m\left(u\frac{\partial p^*}{\partial x} + v\frac{\partial p^*}{\partial y}\right) \tag{3.8}$$

The expression for $c_{pm} = c_p(1 + 0.8q_v)$, where $c_p$ is the specific heat at constant pressure for dry air and $q_v$ is the mixing ratio of water vapor.

### 3.1.4 Hydrostatic Equation

The hydrostatic equation is used to compute the geopotential heights from the virtual temperature $T_v$,

$$\frac{\partial\phi}{\partial ln(\sigma + p_t/p^*)} = -RT_v\left[1 + \frac{q_c + q_r}{1 + q_v}\right]^{-1} \tag{3.9}$$

where $T_v = T(1 + 0.608q_v)$, $q_v$, $q_c$, and $q_r$ are the water vapor, cloud water or ice, and rain water or snow, mixing ratios.

## 3.2 Physics parametrizations

### 3.2.1 Radiation Scheme

RegCM4 uses the radiation scheme of the NCAR CCM3, which is described in *Kiehl et al.* [1996]. Briefly, the solar component, which accounts for the effect of $O_3$, $H_2O$, $CO_2$, and $O_2$, follows the δ-Eddington approximation of *Kiehl et al.* [1996]. It includes 18 spectral intervals from 0.2 to 5 $\mu$m. The cloud scattering and absorption parameterization follow that of *Slingo* [1989], whereby the optical properties of the cloud droplets (extinction optical depth, single scattering albedo, and asymmetry parameter) are expressed in terms of the cloud liquid water content and an effective droplet radius. When cumulus clouds are formed, the gridpoint fractional cloud cover is such that the total cover for the column extending from the model-computed cloud-base level to the cloud-top level (calculated assuming random overlap) is a function of horizontal gridpoint spacing. The thickness of the cloud layer is assumed to be equal to that of the model layer, and a different cloud water content is specified for middle and low clouds.

### 3.2.2 Land Surface Models

**BATS (default):** BATS is a surface package designed to describe the role of vegetation and interactive soil moisture in modifying the surface-atmosphere exchanges of momentum, energy, and water vapor (see *Dickinson et al.* [1993] for details). The model has a vegetation layer, a snow layer, a surface soil layer, 10 cm thick, or root zone layer, 1-2 m thick, and a third deep soil layer 3 m thick. Prognostic equations are solved for the soil layer temperatures using a generalization of the force-restore method of *Deardoff* [1978]. The temperature of the canopy and canopy foilage is calculated diagnostically via an energy balance formulation including sensible, radiative, and latent heat fluxes.

The soil hydrology calculations include predictive equations for the water content of the soil layers. These equations account for precipitation, snowmelt, canopy foiliage drip, evapotranspiration, surface runoff, infiltration below the root zone, and diffusive exchange of water between soil layers. The soil water movement formulation is obtained from a fit to results from a high-resolution soil model *Dickinson* [1984] and the surface runoff rates are expressed as functions of the precipitation rates and the degree of soil water saturation. Snow depth is prognostically calculated from snowfall, snowmelt, and sublimation. Precipitation is assumed to fall in the form of snow if the temperature of the lowest model level is below 271 K.

Sensible heat, water vapor, and momentum fluxes at the surface are calculated using a standard surface drag coefficient formulation based on surface-layer similarity theory. The drag coefficient depends on the surface roughness length and on the atmospheric stability in the surface layer. The surface evapotranspiration rates depend on the availability of soil water. Biosphere-Atmosphere Transfer Scheme (BATS) has 20 vegetation types (Table 3.2; soil textures ranging from coarse (sand), to intermediate (loam), to fine (clay); and different soil colors (light to dark) for the soil albedo calculations. These are described in *Dickinson et al.* [1986].

In the latest release version, additional modifications have been made to BATSin order to account for the subgrid variability of topography and landcover using a mosaic-type approach [*Giorgi et al.*, 2003a]. Thismodification adopts a regular fine-scale surface subgrid for eachcoarse model grid cell. Meteorological variables are disaggregatedfrom the coarse grid to the fine grid based on the elevationdifferences. The BATS calculations are then performed separatelyfor each subgrid cell, and surface fluxes are reaggregated onto thecoarse grid cell for input to the atmospheric model. This parameterization showed a marked improvement in the representation ofthe surface hydrological cycle in mountainous regions [*Giorgi et al.*, 2003a]. As a first augmentation, in REGional Climate Model version 4 (RegCM4) two new land use types were added to BATS to represent urban and sub-urban environments. Urban development not only modifies the surface albedo and alters the surface energy balance, but also creates impervious surfaces with large effects on runoff and evapotranspiration. These effects can be described by modifying relevant properties of the land surface types in the BATS package, such as maximum vegetation cover, roughness length, albedo, and soil characteristics. For this purpose, we implemented the parameters proposed in Table 1 of *Kueppers et al.* [2008].

**CLM (optional):** The Community Land Model (CLM; *Oleson et al.* [2008]) is the land surface model developed by the National Center of Atmospheric Research (NCAR) as part of the Community Climate System Model (CCSM), described in detail in *Collins et al.* [2006]. CLM version 3.5 was coupled to RegCM for a more detailed land surface description option. CLM contains five possible snow layers with an additional representation of trace snow and ten unevenly spaced soil layers with explicit solutions of temperature, liquid water and ice water in each layer. To account for land surface complexity within a climate model grid cell, CLM uses a tile or mosaic approach

Table 3.1: Land Cover/Vegetation classes

| | |
|---|---|
| 1. | Crop/mixed farming |
| 2. | Short grass |
| 3. | Evergreen needleleaf tree |
| 4. | Deciduous needleleaf tree |
| 5. | Deciduous broadleaf tree |
| 6. | Evergreen broadleaf tree |
| 7. | Tall grass |
| 8. | Desert |
| 9. | Tundra |
| 10. | Irrigated Crop |
| 11. | Semi-desert |
| 12. | Ice cap/glacier |
| 13. | Bog or marsh |
| 14. | Inland water |
| 15. | Ocean |
| 16. | Evergreen shrub |
| 17. | Deciduous shrub |
| 18. | Mixed Woodland |
| 19. | Forest/Field mosaic |
| 20. | Water and Land mixture |

to capture surface heterogeneity. Each CLM gridcell contains up to four different land cover types (glacier, wetland, lake, and vegetated), where the vegetated fraction can be further divided into 17 different plant functional types. Hydrological and energy balance equations are solved for each land cover type and aggregated back to the gridcell level. A detailed discussion of CLM version 3 implemented in RegCM3 and comparative analysis of land surface parameterization options is presented in *Steiner et al.* [2009]. Since CLM was developed for the global scale, several input files and processes were modified to make it more appropriate for regional simulations, including (1) the use of high resolution input data, (2) soil moisture initialization, and (3) and an improved treatment of grid cells along coastlines. For the model input data, CLM requires several time-invariant surface input parameters: soil color, soil texture, percent cover of each land surface type, leaf and stem area indices, maximum saturation fraction, and land fraction [*Lawrence and Chase*, 2007]. Table 3.3 shows the resolution for each input parameter used at the regional scale in RegCM-CLM compared to resolutions typically used for global simulations. The resolution of surface input parameters was increased for several parameters to capture surface heterogeneity when interpolating to the regional climate grid. Similar to *Lawrence and Chase* [2007], the number of soil colors was extended from 8 to 20 classes to resolve regional variations. The second modification was to update the soil moisture initialization based on a climatological soil moisture average [*Giorgi and Bates*, 1989] over the use of constant soil moisture content throughout the grid generally used for global CLM. By using a climatological average for soil moisture, model spin-up time is reduced with regards to deeper soil layers. The third modification to the CLM is the inclusion of a mosaic approach for gridcells that contain both land and ocean surface types. With this approach, a weighted average of necessary surface variables was calculated for land/ocean gridcells using the land fraction input dataset. This method provides a better representation of coastlines using the high-resolution land fraction data described in Table 3.3. For a more detailed description of CLM physics parameterizations see *Oleson* [2004].

Table 3.2: BATS vegetation/land-cover

| Parameter | Land Cover/Vegetation Type | | | | | | | | | | | | | | | | | | | |
|---|---|---|---|---|---|---|---|---|---|---|---|---|---|---|---|---|---|---|---|---|
| | 1 | 2 | 3 | 4 | 5 | 6 | 7 | 8 | 9 | 10 | 11 | 12 | 13 | 14 | 15 | 16 | 17 | 18 | 19 | 20 |
| Max fractional vegetation cover | 0.85 | 0.80 | 0.80 | 0.80 | 0.80 | 0.90 | 0.80 | 0.00 | 0.60 | 0.80 | 0.35 | 0.00 | 0.80 | 0.00 | 0.00 | 0.80 | 0.80 | 0.80 | 0.80 | 0.80 |
| Difference between max fractional vegetation cover and cover at 269 K | 0.6 | 0.1 | 0.1 | 0.3 | 0.5 | 0.3 | 0.0 | 0.2 | 0.6 | 0.1 | 0.0 | 0.4 | 0.0 | 0.0 | 0.2 | 0.3 | 0.2 | 0.4 | 0.4 | |
| Roughness length (m) | 0.08 | 0.05 | 1.00 | 1.00 | 0.80 | 2.00 | 0.10 | 0.05 | 0.04 | 0.06 | 0.10 | 0.01 | 0.03 | 0.0004 | 0.0004 | 0.10 | 0.10 | 0.80 | 0.3 | 0.3 |
| Displacement height (m) | 0.0 | 0.0 | 9.0 | 9.0 | 0.0 | 18.0 | 0.0 | 0.0 | 0.0 | 0.0 | 0.0 | 0.0 | 0.0 | 0.0 | 0.0 | 0.0 | 0.0 | 0.0 | 0.0 | 0.0 |
| Min stomatal resistence (s/m) | 45 | 60 | 80 | 80 | 120 | 60 | 60 | 200 | 80 | 45 | 150 | 200 | 45 | 200 | 200 | 80 | 120 | 100 | 120 | 120 |
| Max Leaf Area Index | 6 | 2 | 6 | 6 | 6 | 6 | 6 | 0 | 6 | 6 | 6 | 0 | 6 | 0 | 0 | 6 | 6 | 6 | 6 | 6 |
| Min Leaf Area Index | 0.5 | 0.5 | 5 | 1 | 1 | 5 | 0.5 | 0 | 0.5 | 0.5 | 0.5 | 0 | 0.5 | 0 | 0 | 5 | 1 | 3 | 0.5 | 0.5 |
| Stem (dead matter area index) | 0.5 | 4.0 | 2.0 | 2.0 | 2.0 | 2.0 | 2.0 | 0.5 | 0.5 | 2.0 | 2.0 | 2.0 | 2.0 | 2.0 | 2.0 | 2.0 | 2.0 | 2.0 | 2.0 | 2.0 |
| Inverse square root of leaf dimension ($m^{-1/2}$) | 10 | 5 | 5 | 5 | 5 | 5 | 5 | 5 | 5 | 5 | 5 | 5 | 5 | 5 | 5 | 5 | 5 | 5 | 5 | 5 |
| Light sensitivity factor ($m^2$ $W^{-1}$) | 0.02 | 0.02 | 0.06 | 0.06 | 0.06 | 0.06 | 0.02 | 0.02 | 0.02 | 0.02 | 0.02 | 0.02 | 0.02 | 0.02 | 0.02 | 0.02 | 0.02 | 0.06 | 0.02 | 0.02 |
| Upper soil layer depth (mm) | 100 | 100 | 100 | 100 | 100 | 100 | 100 | 100 | 100 | 100 | 100 | 100 | 100 | 100 | 100 | 100 | 100 | 100 | 100 | 100 |
| Root zone soil layer depth (mm) | 1000 | 1000 | 1500 | 1500 | 2000 | 1500 | 1000 | 1000 | 1000 | 1000 | 1000 | 1000 | 1000 | 1000 | 1000 | 1000 | 1000 | 2000 | 2000 | 2000 |
| Depth of total soil (mm) | 3000 | 3000 | 3000 | 3000 | 3000 | 3000 | 3000 | 3000 | 3000 | 3000 | 3000 | 3000 | 3000 | 3000 | 3000 | 3000 | 3000 | 3000 | 3000 | 3000 |
| Soil texture type | 6 | 6 | 6 | 6 | 7 | 8 | 6 | 3 | 6 | 6 | 5 | 12 | 6 | 6 | 6 | 6 | 5 | 6 | 6 | 0 |
| Soil color type | 5 | 3 | 4 | 4 | 4 | 4 | 4 | 1 | 3 | 3 | 2 | 1 | 5 | 5 | 5 | 4 | 3 | 4 | 4 | 0 |
| Vegetation albedo for wavelengths $< 0.7\ \mu$m | 0.10 | 0.10 | 0.05 | 0.05 | 0.08 | 0.04 | 0.08 | 0.20 | 0.10 | 0.08 | 0.17 | 0.80 | 0.06 | 0.07 | 0.07 | 0.05 | 0.08 | 0.06 | 0.06 | 0.06 |
| Vegetation albedo for wavelengths $> 0.7\ \mu$m | 0.30 | 0.30 | 0.23 | 0.23 | 0.28 | 0.20 | 0.30 | 0.40 | 0.30 | 0.28 | 0.34 | 0.60 | 0.18 | 0.20 | 0.20 | 0.23 | 0.28 | 0.24 | 0.18 | 0.18 |

Table 3.3: Resolution for CLM input parameters

| Input data | Grid Spacing | Lon range | Lat range |
|---|---|---|---|
| Glacier | 0.05° x 0.05° | ±179.975 | ±89.975 |
| Lake | 0.05° x 0.05° | ±179.975 | ±89.975 |
| Wetland | 0.05° x 0.05° | ±179.975 | ±89.975 |
| Land fraction | 0.05° x 0.05° | ±179.975 | ±89.975 |
| LAI/SAI | 0.5° x 0.5° | ±179.75 | ±89.75 |
| PFT | 0.5° x 0.5° | ±179.75 | ±89.75 |
| Soil color | 0.05° x 0.05° | ±179.975 | ±89.975 |
| Soil texture | 0.05° x 0.05° | ±179.975 | ±89.975 |
| Max. sat. area | 0.5° x 0.5° | ±179.75 | ±89.75 |

### 3.2.3 Planetary Boundary Layer Scheme

**Holtslag PBL**

The Holtslag planetary boundary layer scheme, developed by *Holtslag et al.* [1990], is based on a nonlocal diffusion concept that takes into account countergradient fluxes resulting from large-scale eddies in an unstable, well-mixed atmosphere. The vertical eddy flux within the PBL is given by

$$F_c = -K_c \left( \frac{\partial C}{\partial z} - \gamma_c \right) \tag{3.10}$$

where $\gamma_c$ is a "countergradient" transport term describing nonlocal transport due to dry deep convection. The eddy diffusivity is given by the nonlocal formulation

$$K_c = k w_t z \left( 1 - \frac{z}{h}^2 \right) \tag{3.11}$$

where $k$ is the von Karman constant; $w_t$ is a turbulent convective velocity that depends on the friction velocity, height, and the Monin–Obhukov length; and $h$ is the PBL height.

The countergradient term for temperature and water vapor is given by

$$\gamma_c = C \frac{{\phi_c}^0}{w_t h} \tag{3.12}$$

where C is a constant equal to 8.5, and ${\phi_c}^0$ is the surface temperature or water vapor flux. Equation 3.12 is applied between the top of the PBL and the top of the surface layer, which is assumed to be equal to $0.1h$. Outside this region and for momentum, $\gamma_c$ is assumed to be equal to 0.

For the calculation of the eddy diffusivity and countergradient terms, the PBL height is diagnostically computed from

$$h = \frac{\mathrm{R_{icr}}[u(h)^2 + v(h)^2]}{(g/\theta_s)[\theta_v(h) - \theta_s]} \tag{3.13}$$

where $u(h)$, $v(h)$, and $\theta_v$ are the wind components and the virtual potential temperature at the PBL height, $g$ is gravity, $\mathrm{R_{icr}}$ is the critical bulk Richardson number, and $\theta_s$ is an appropriate temperature of are near the surface. Refer to *Holtslag et al.* [1990] and *Holtslag and Boville* [1993] for a more detailed description.

Compared to other schemes this formulation tends to produce relatively strong, and often excessive, turbulent vertical transfer. For example, after extensive testing, we found excessive vertical transfer of moisture in the model resulting in low moisture amounts near the surface and excessive moisture near the PBL top.

Therefore in order to ameliorate this problem, the countergradient term for water vapor was removed in RegCM4. Another problem of the Holtslag scheme (at least in our implementation) is an excessive vertical transport of heat, moisture and momentum in very stable conditions, such as during the winter in northern hemisphere high latitude regions. For example we found that in such conditions the scheme fails to simulate near surface temperature inversions.

This in turn leads to large warm winter biases (even ¿ 10 degrees) over regions such as Northern Siberia and Northern Canada. As an ad-hoc fix to address this problem, in RegCM4 we implemented the following modification to the scheme:

- We first define very stable conditions within the Holtslag parameterization as conditions in which the ratio of the height from the surface over the Monin-Obhukov length is lower than 0.1.
- When such conditions are found, we set to 0 the eddy diffusivity and counter-gradient terms for all variables.

Preliminary tests showed that this modification reduces the warm bias in high latitude winter conditions and allows the model to better capture surface inversions. These modifications have thus been incorporated as default in the RegCM4 code.

**The UW Turbulence Closure Model**

As an alternative to the Holtslag PBL, the University of Washington turbulence closure model [*Grenier and Bretherton*, 2001; *Bretherton et al.*, 2004] has been coupled to RegCM. The development of this coupling, and its validation for western North America, is described by *O'Brien et al.* [2012], and validation over Europe is described by *Güttler et al.* [2013]. This parameterization was originally implemented to allow RegCM to simulate stratocumulus and coastal fog [*O'Brien et al.*, 2012; *OBrien et al.*, 2012].

The UW model is a 1.5-order, local, down-gradient diffusion parametrization. It will be referred to as a PBL model, but it has capabilities that allow it to calculate vertical fluxes out side of the PBL as well as within; *Bretherton et al.* [2004] refers to it as a moist turbulence parametrization. As with other $1^{st}$-order models, such as the Holtslag model, the UW model parameterizes turbulent fluxes as the product of a diffusivity and a gradient. In contrast to $1^{st}$-order models, however, the model prognostically determines the turbulent kinetic energy (TKE, also referred to as $e$), and it uses TKE to define the diffusivites.

As with the Holtslag mode, diffusivity is defined as the product of a length scale and a velocity scale, though the velocity scale is defined as the square root of local TKE rather than the convective velocity scale. The length scale is the UW model's master length scale, either $l = \kappa z$ or $l = kz/(1+kz/\lambda)$ (this can be set in the RegCM configuration file), multiplied by a correction factor that depends on local stability[1], and the velocity scale is the square root of twice the TKE.

The boundary layer height in the UW model is defined as the first level where the expression $N(z)^2 l(z)^2$ (where $N$ is the Brunt-Väisälä frequency, $N^2 = \frac{g}{\theta_v}\frac{\partial \theta_v}{\partial z}$) exceeds half of the negative of its layer-mean value. Since the flux of buoyancy, $b$, can be written as $\overline{w'b'} = -K_h \frac{\partial b}{\partial z}$, and it can be shown that $N^2 = \frac{\partial b}{\partial z}$, $N^2$ can be viewed as being proportional to the local buoyancy flux in the UW model. In this interpretation, this condition for PBL top (or the top of any turbulent layer) can be approximately viewed as a "condition that the buoyancy flux anywhere in the interior of a convective layer not be more negative than -0.5 of the layer-mean buoyancy flux" [*Bretherton et al.*, 2004]. In other words for an unstable PBL, the PBL ends approximately when the virtual potential temperature profile becomes so stable that the buoyancy flux is opposite to and half as strong as the mean buoyancy flux below. This condition for the height of the PBL can be encapsulated in the following implicit equation, where the $z$ and $h$ values are restricted to lie on the model's vertical grid:

$$N^2(h)l^2(h) = -\frac{1}{2}\frac{1}{h}\int_0^h N^2(z)l^2(z)\cdot dz \tag{3.14}$$

The diffusivity of scalar quantities and momentum at a given height, $z$, are given as $K_{h,m}(z) = l(z)S_{h,m}(z)\sqrt{2e}$. The TKE budget equation is solved at each time step according to equation 3.15 (where the shear frequency, $S_f = \sqrt{(\frac{\partial u}{\partial z})^2 + (\frac{\partial v}{\partial z})^2}$), which is the balance of buoyancy ($B$), shear ($S$), transport ($T$), and dissipation ($D$) terms. Following *Grenier and Bretherton* [2001], the TKE diffusivity, $K_e$, is set as 5 times the eddy diffusivity, $K_m$. The

[1]The correction factors are called the stability functions $S_{h,m}$, which are defined in *Galperin et al.* [1988]

RegCM dynamical core has been modified to account for horizontal transport (i.e. advection and diffusion) of TKE when the UW model is active.

$$\frac{\partial e}{\partial t}\Big|_{BL} = -K_h N^2 + K_m {S_f}^2 + \frac{\partial}{\partial z}[K_e \frac{\partial e}{\partial z}] - \frac{e^{\frac{3}{2}}}{l} \tag{3.15a}$$

$$\frac{\partial e}{\partial t}\Big|_{BL} = B + S + T - D \tag{3.15b}$$

The UW model treats TKE and diffusivity at the surface and the PBL top specially. At the surface, TKE is diagnosed as $e_0 = Bu_*^2$, where $B$ is a constant. At the PBL top (the temperature inversion), diffusivity for all quantities is set as $K_X = w_e \Delta_{inv} z$. The entrainment flux, which uses the Turner-Deardorff formulation, is set as $w_e = \frac{AU}{R_i}$, where $A$ is the entrainment efficiency[2], $U$ is a scale velocity, and $R_i$ is a bulk Richardson number. The UW model specifies the bulk Richardson number as $R_i = \frac{L\Delta b}{U^2}$, with $U = \sqrt{e_{inv}}$, and $L = l$ as the master length scale. It is assumed that the PBL does not entrain or detrain TKE.

The UW model accounts for the production of turbulence by cloud-top radiative cooling, which is a critical difference from the Holtslag PBL. If a turbulent layer (e.g. the PBL) is cloud-topped, then a term is added to the TKE budget equation: $\frac{\partial e}{\partial t}\Big|_{RAD} = \frac{g\Delta F_{lw}}{C_p \rho \Gamma \theta_v}|_{inv}$, where $\Delta F_{lw}$ is the jump in long-wave flux at cloud-top. This term is crucial for ensuring that turbulence is produced in the otherwise-stable regions where stratocumulus exist.

The UW model is written specifically to deal with moist thermodynamic processes (i.e. mixing between clear and cloudy air): its core prognostic equations are written to predict liquid water potential temperature, $\theta_l$, total water mixing ratio, $Q$, and momentum, $u_i$. The use of these variables ensures that enthalpy and water are explicitly conserved when mixing between clear and cloudy parcels of air; care has to be taken otherwise (when using $\theta$ and $q$) to ensure conservation in this situation.

At each model timestep, the UW model does the following: determines the boundary layer height, $h$, calculates the surface TKE,predicts the change in TKE due to PBL processes, determines the diffusivities at each height, and predicts the change in each prognostic quantity due to vertical convergence of turbulent fluxes. The full set of equations that the UW PBL model solves at each time step, including equations 3.14 and 3.15, follows:

$$\frac{\partial u_i}{\partial t}\Big|_{BL} = \frac{\partial}{\partial z}[\kappa z S_m(z) \sqrt{2e(z)} \frac{\partial u_i}{\partial z}] \tag{3.16a}$$

$$\frac{\partial \theta_l}{\partial t}\Big|_{BL} = \frac{\partial}{\partial z}[\kappa z S_h(z) \sqrt{2e(z)} \frac{\partial \theta_l}{\partial z}] \tag{3.16b}$$

$$\frac{\partial Q}{\partial t}\Big|_{BL} = \frac{\partial}{\partial z}[\kappa z S_h(z) \sqrt{2e(z)} \frac{\partial Q}{\partial z}] \tag{3.16c}$$

$$\frac{\partial \chi_j}{\partial t}\Big|_{BL} = \frac{\partial}{\partial z}[\kappa z S_h(z) \sqrt{2e(z)} \frac{\partial \chi_j}{\partial z}] \tag{3.16d}$$

### 3.2.4 Convective Precipitation Schemes

Convective precipitation is computed using one of three schemes: (1) Modified-Kuo scheme *Anthes* [1977]; (2) Grell scheme *Grell* [1993]; and (3) MIT-Emanuel scheme [*Emanuel*, 1991; *Emanuel and Zivkovic-Rothman*, 1999]. In addition, the Grell parameterization is implemented using one of two closure assumptions: (1) the Arakawa and Schubert closure *Grell et al.* [1994] and (2) the Fritsch and Chappell closure *Fritsch and Chappell* [1980], hereafter refered to as AS74 and FC80, respectively.

1. **Kuo Scheme:** Convective activity in the Kuo scheme is initiated when the moisture convergence $M$ in a column exceeds a given threshold and the vertical sounding is convectively unstable. A fraction of the moisture convergence $\beta$ moistens the column and the rest is converted into rainfall $P^{CU}$ according to the following relation:

[2]The entrainment efficiency is partially determined by the mixture of clear and cloudy air that happens at the inversion top: *Grenier and Bretherton* [2001] takes special care to develop a parametrization for A that includes 'evaporative enhancement' effects for cases when a cloudy-clear mixture of air is more dense than its surroundings.

$$P^{CU} = M(1-\beta). \tag{3.17}$$

$\beta$ is a function of the average relative humidity $\overline{RH}$ of the sounding as follows:

$$\beta = \left\{ \begin{array}{ll} 2(1-\overline{RH}) & \overline{RH} \geq 0.5 \\ 1.0 & \text{otherwise} \end{array} \right\} \tag{3.18}$$

Note that the moisture convergence term includes only the advective tendencies for water vapor. However, evapotranspiration from the previous time step is indirectly included in $M$ since it tends to moisten the lower atmosphere. Hence, as the evapotranspiration increases, more and more of it is converted into rainfall assuming the column is unstable. The latent heating resulting from condensation is distributed between the cloud top and bottom by a function that allocates the maximum heating to the upper portion of the cloud layer. To eliminate numerical point storms, a horizontal diffusion term and a time release constant are included so that the redistributions of moisture and the latent heat release are not performed instantaneously [*Giorgi and Bates*, 1989; *Giorgi and Marinucci*, 1991].

2. **Grell Scheme:** The Grell scheme *Grell* [1993], similar to the AS74 parameterization, considers clouds as two steady-state circulations: an updraft and a downdraft. No direct mixing occurs between the cloudy air and the environmental air except at the top and bottom of the circulations. The mass flux is constant with height and no entrainment or detrainment occurs along the cloud edges. The originating levels of the updraft and downdraft are given by the levels of maximum and minimum moist static energy, respectively. The Grell scheme is activated when a lifted parcel attains moist convection. Condensation in the updraft is calculated by lifting a saturated parcel. The downdraft mass flux ($m_0$) depends on the updraft mass flux ($m_b$) according to the following relation:

$$m_0 = \frac{\beta I_1}{I_2} m_b \tag{3.19}$$

where $I_1$ is the normalized updraft condensation, $I_2$ is the normalized downdraft evaporation, and $\beta$ is the fraction of updraft condensation that re-evaporates in the downdraft. $\beta$ depends on the wind shear and typically varies between 0.3 and 0.5. Rainfall is given by

$$P^{CU} = I_1 m_b (1-\beta) \tag{3.20}$$

Heating and moistening in the Grell scheme are determined both by the mass fluxes and the detrainment at the cloud top and bottom. In addition, the cooling effect of moist downdrafts is included.

Due to the simplistic nature of the Grell scheme, several closure assumptions can be adopted. RegCM4's earlier version directly implements the quasi-equilibrium assumption of AS74. It assumes that convective clouds stabilize the environment as fast as non-convective processes destabilize it as follows:

$$m_b = \frac{ABE'' - ABE}{NA\Delta t} \tag{3.21}$$

where $ABE$ is the buoyant energy available for convection, $ABE''$ is the amount of buoyant energy available for convection in addition to the buoyant energy generated by some of the non-convective processes during the time interval $\Delta t$, and $NA$ is the rate of change of $ABE$ per unit $m_b$. The difference $ABE'' - ABE$ can be thought of as the rate of destabilization over time $\Delta t$. $ABE''$ is computed from the current fields plus the future tendencies resulting from the advection of heat and moisture and the dry adiabatic adjustment.

In the latest RegCM4 version, by default, we use a stability based closure assumption, the FC80 type closure assumption, that is commonly implemented in GCMs and RCMs. In this closure, it is assumed that convection removes the *ABE* over a given time scale as follows:

$$m_b = \frac{ABE}{NA\tau} \tag{3.22}$$

where $\tau$ is the *ABE* removal time scale.

The fundamental difference between the two assumptions is that the AS74 closure assumption relates the convective fluxes and rainfall to the tendencies in the state of the atmosphere, while the FC80 closure assumption relates the convective fluxes to the degree of instability in the atmosphere. Both schemes achieve a statistical equilibrium between convection and the large-scale processes.

A number of parameters present in the scheme can be used to optimize its performance, and *Giorgi et al.* [1993c] discusses a wide range of sensitivity experiments. We found that the parameter to which the scheme is most sensitive is by and large the fraction of precipitation evaporated in the downdraft (Peff, with values from 0 to 1), which essentially measures the precipitation efficiency. Larger values of Peff lead to reduced precipitation.

3. **MIT-Emanuel scheme:** More detailed descriptions can be found in *Emanuel* [1991] and*Emanuel and Zivkovic-Rothman* [1999]. The scheme assumes that the mixing in clouds ishighly episodic and inhomogeneous (as opposed to a continuousentraining plume) and considers convective fluxes based on anidealized model of sub-cloud-scale updrafts and downdrafts.Convection is triggered when the level of neutral buoyancy is greaterthan the cloud base level. Between these two levels, air is liftedand a fraction of the condensed moisture forms precipitation while theremaining fraction forms the cloud. The cloud is assumed to mix withthe air from the environment according to a uniform spectrum ofmixtures that ascend or descend to their respective levels of neutralbuoyancy. The mixing entrainment and detrainment rates are functionsof the vertical gradients of buoyancy in clouds. The fraction of thetotal cloud base mass flux that mixes with its environment at eachlevel is proportional to the undiluted buoyancy rate of change withaltitude. The cloud base upward mass flux is relaxed towards thesub-cloud layer quasi equilibrium.

   In addition to a more physical representation of convection, the MIT-Emanuel scheme offers several advantages compared to theother RegCM4 convection options. For instance, it includes aformulation of the auto-conversion of cloud water into precipitationinside cumulus clouds, and ice processes are accounted for by allowingthe auto-conversion threshold water content to be temperaturedependent. Additionally, the precipitation is added to a single,hydrostatic, unsaturated downdraft that transports heat and water. Lastly, the MIT-Emanuel scheme considers the transport of passive tracers.

   The MIT scheme is the most complex of the three and also includes a number of parameters that can be used to optimize the model performance in different climate regimes. Differently from the Grell scheme, however, test experiments did not identify a single parameter to which the model is most sensitive.

A major augmentation in RegCM4 compared to previous versions of the model is the capability of running different convection schemes over land and ocean, a configuration which we refer to as mixed convection. Extensive test experiments showed that different schemes have different performance over different regions, and in particular over land vs. ocean areas.

For example, the MIT scheme tends to produce excessive precipitation over land areas, especially through the occurrence of very intense individual precipitation events.

In other words, once the scheme is activated, it becomes difficult to decelerate. Conversely, we found that the Grell scheme tends to produce excessively weak precipitation over tropical oceans.

These preliminary tests suggested that a mixed convection approach by which, for example, the MIT scheme is used over oceans and the Grell scheme over land, might be the most suitable option to pursue, and therefore this option was added to the model.

### 3.2.5 Large-Scale Precipitation Scheme

Subgrid Explicit Moisture Scheme (SUBEX) is used to handle nonconvective clouds and precipitation resolved by the model. This is one of the new components of the model. SUBEX accounts for the subgrid variability in

clouds by linking the average grid cell relative humidity to the cloud fraction and cloud water following the work of *Sundqvist et al.* [1989].

The fraction of the grid cell covered by clouds, $FC$, is determined by,

$$FC = \sqrt{\frac{RH - RH_{min}}{RH_{max} - RH_{min}}} \tag{3.23}$$

where $RH_{min}$ is the relative humidity threshold at which clouds begin to form, and $RH_{max}$ is the relative humidity where $FC$ reaches unity. $FC$ is assumed to be zero when RH is less than $RH_{min}$ and unity when RH is greater than $RH_{max}$.

Precipitation $P$ forms when the cloud water content exceeds the autoconversion threshold ${Q^{th}}_c$ according to the following relation:

$$P = C_{ppt}(Q_c/FC - {Q_c}^{th})FC \tag{3.24}$$

where $1/C_{ppt}$ can be considered the characteristic time for which cloud droplets are converted to raindrops. The threshold is obtained by scaling the median cloud liquid water content equation according to the following:

$${Q^{th}}_c = C_{acs}10^{-0.49+0.013T} \tag{3.25}$$

where $T$ is temperature in degrees Celsius, and $C_{acs}$ is the autoconversion scale factor. Precipitation is assumed to fall instantaneously.

SUBEX also includes simple formulations for raindrop accretion and evaporation. The formulation for the accretion of cloud droplets by falling rain droplets is based on the work of *Beheng* [1994] and is as follows:

$$P_{acc} = C_{acc}QP_{sum} \tag{3.26}$$

where $P_{acc}$ is the amount of accreted cloud water, $C_{acc}$ is the accretion rate coefficient, and $P_{sum}$ is the accumulated precipitation from above falling through the cloud.

Precipitation evaporation is based on the work of *Sundqvist et al.* [1989] and is as follows

$$P_{evap} = C_{evap}(1 - RH){P^{1/2}}_{sum} \tag{3.27}$$

where $P_{evap}$ is the amount of evaporated precipitation, and $C_{evap}$ is the rate coefficient. For a more detailed description of SUBEX and a list of the parameter values refer to *Pal et al.* [2000].

Traditionally, REGional Climate Model version 3 (RegCM3) has shown a tendency to produce excessive precipitation, especially at high resolutions, and optimizations of the in-cloud liquid water threshold for the activation of the autoconversion term *Qcth* and the rate of sub-cloud evaporation *Cevap* parameters have proven effective in ameliorating this problem: greater values of *Qth* and *Cevap* lead to decreased precipitation amounts.

### 3.2.6 Ocean flux Parameterization

BATS uses standard Monin-Obukhov similarity relations to compute the fluxes with no special treatment of convective and very stable conditions. In addition, the roughness length is set to a constant, i.e. it is not a function of wind and stability.

The Zeng scheme describes all stability conditions and includes a gustiness velocity to account for the additional flux induced by boundary layer scale variability. Sensible heat (SH), latent heat (LH), and momentum ($\tau$) fluxes between the sea surface and lower atmosphere are calculated using the following bulk aerodynamic algorithms,

$$\tau = \rho_a {u_*}^2({u_x}^2 + {u_y}^2)^{1/2}/u \tag{3.28}$$

$$\mathrm{SH} = -\rho_a C_{pa} u_* \theta_* \tag{3.29}$$

$$\mathrm{LH} = -\rho_a L_e u_* q_* \tag{3.30}$$

where $u_x$ and $u_y$ are mean wind components, $u_*$ is the frictional wind velocity, $\theta_*$ is the temperature scaling parameter, $q_*$ is the specific humidity scaling parameter, $\rho_a$ is air density, $C_{pa}$ is specific heat of air, and $L_e$ is the latent heat of vaporization. For further details on the calculation of these parameters refer to *Zeng et al.* [1998].

### 3.2.7 Prognostic Sea Surface Skin Temperature Scheme

By default in RegCM, sea surface temperatures (SST) are prescribed every six hours from temporally interpolated weekly or monthly SST products. These products, which are produced from satellite retrievals and in situ measurements, are representative of the mean temperature in the top few meters of the ocean. However, the actual SST can differ significantly from this mean temperature due to the cool-skin and warm-layer effects described by *Fairall et al.* [1996]. To improve the calculation of diurnal fluxes over the ocean, the prognostic SST scheme described by *Zeng* [2005] was implemented in RegCM4. The scheme is based on a two-layer one-dimensional heat transfer model, with the top layer representing the upper few millimeters of the ocean which is cooled by net longwave radiation loss and surface fluxes. The bottom layer is three meters thick, it is warmer by solar radiation and exchanges heat with the top layer. This diurnal SST scheme appears to provide significant, although not major, effects on the model climatology mostly over tropical oceans, for example the Indian ocean, and it is now used as default in RegCM4.

### 3.2.8 Pressure Gradient Scheme

Two options are available for calculating the pressure gradient force. The normal way uses the full fields. The other way is the hydrostatic deduction scheme which makes use of a perturbation temperature. In this scheme, extra smoothing on the top is done in order to reduce errors related to the PGF calculation.

### 3.2.9 Lake Model

The lake model developed by *Hostetler et al.* [1993] can be interactively coupled to the atmospheric model. In the lake model, fluxes of heat, moisture, and momentum are calculated based on meteorological inputs and the lake surface temperature and albedo. Heat is transferred vertically between lake model layers by eddy and convective mixing. Ice and snow may cover part or all of the lake surface.

In the lake model, the prognostic equation for temperature is

$$\frac{\partial T}{\partial t} = (k_e + k_m)\frac{\partial^2 T}{\partial z^2} \tag{3.31}$$

where $T$ is the temperature of the lake layer, and $k_e$ and $k_m$ are the eddy and molecular diffusivities, respectively. The parameterization of *Henderson-Sellers* [1986] is used to calculate $k_e$ and $k_m$ is set to a constant value of $39 \times 10^{-7}\ m^2\ s^{-1}$ except under ice and at the deepest points in the lake.

Sensible and latent heat fluxes from the lake are calculated using the BATS parameterizations *Dickinson et al.* [1993]. The bulk aerodynamic formulations for latent heat flux ($F_q$) and sensible heat flux ($F_s$) are as follows,

$$F_q = \rho_a C_D V_a (q_s - q_a) \tag{3.32}$$
$$F_s = \rho_a C_p C_D V_a (T_s - T_a) \tag{3.33}$$

where the subscripts $s$ and $a$ refer to surface and air, respectively; $\rho_a$ is the density of air, $V_a$ is the wind speed, $C_p$, $q$ is specific humidity, and $T$ is temperature. The momentum drag coefficient, $C_D$, depends on roughness length and the surface bulk Richardson number.

Under ice-free conditions, the lake surface albedo is calculated as a function of solar zenith angle *Henderson-Sellers* [1986]. Longwave radiation emitted from the lake is calculated according to the Stefan-Boltzmann law. The lake model uses the partial ice cover scheme of *Patterson and Hamblin* [1988] to represent the different heat and moisture exchanges between open water and ice surfaces and the atmosphere, and to calculate the surface energy of lake ice and overlying snow. For further details refer to *Hostetler et al.* [1993] and *Small and Sloan* [1999].

### 3.2.10 Aerosols and Dust (Chemistry Model)

The representation of dust emission processes is a key element in a dust model and depends on the wind conditions, the soil characteristics and the particle size. Following *Laurent et al.* [2008] and *Alfaro and Gomes* [2001], here the dust emission calculation is based on parameterizations of soil aggregate saltation and sandblasting processes. The main steps in this calculation are: The specification of soil aggregate size distribution for each model grid cell, the calculation of a threshold friction velocity leading to erosion and saltation processes, the calculation of the horizontal saltating soil aggregate mass flux, and finally the calculation of the vertical transportable dust particle mass flux generated by the saltating aggregates. In relation to the BATS interface, these parameterizations become effective in the model for cells dominated by desert and semi desert land cover.

# Chapter 4

# Future Developments

We have lot of exciting plans for future model improvements, some of which are in a already mature stage and under testing, with some published results, whereas others are done only on the paper in a whishlist for next years. Nevertheless we want to share this with users, to have hints and encourage contributions. Some of the development results/ideas are listed below, in a ”time to market” order.

## 4.1 Tiedtke convection scheme

Adrian Tompkins is developing an adaptation of the ECMWF 38R2 *Tiedtke* [1989] cumulus convection scheme for the RegCM model.

## 4.2 Semi-Lagrangian dynamic core

A semi-Lagrangian advection scheme for the water vapor and advection tracers will allow a different timestep for the transport schemes, which should result in a performance prize.

## 4.3 Non-Hydrostatic core

We want to implement the non-hydrostatic core to allow physical downscaling of large scale model simulation under the 20 kilometers limit of the hydrostatic model.

# Bibliography


Alfaro, S. C., and L. Gomes, Modeling mineral aerosol production by wind erosion: Emission intensities and aerosol size distributions in source areas, *Journal of Geophysical Research, 106*, d16, 2001.

Anthes, R. A., A cumulus parameterization scheme utilizing a one-dimensional cloud model, *Mon. Wea. Rev., 105*, 270–286, 1977.

Beheng, K. D., A parameterization of warm cloud microphysical conversion processes, *Atmos. Res., 33*, 193–206, 1994.

Bretherton, C. S., J. McCaa, and H. Grenier, A new parameterization for shallow cumulus convection and its application to marine subtropical cloud-topped boundary layers. part i: Description and 1d results, *Monthly Weather Review, 132*, 864–882, 2004.

Briegleb, B. P., Delta-eddington approximation for solar radiation in the ncar community climate model, *J. Geophys. Res., 97*, 7603–7612, 1992.

Collins, W. D., et al., The Community Climate System Model version 3 (CCSM3), *Journal of Climate, 19*, 2122–2143, 2006.

Deardoff, J. W., Efficient prediction of ground surface temperature and moisture with inclusion of a layer of vegetation, *J. Geophys. Res., 83*, 1889–1903, 1978.

Dickinson, R. E., *Climate Processes and Climate Sensitivity*, chap. Modeling evapotranspiration processes for three-dimensional global climate models, pp. 52–72, American Geophysical Union, 1984.

Dickinson, R. E., P. J. Kennedy, A. Henderson-Sellers, and M. Wilson, Biosphere-atmosphere transfer scheme (bats) for the ncar community climate model, *Tech. Rep. NCARE/TN-275+STR*, National Center for Atmospheric Research, 1986.

Dickinson, R. E., R. M. Errico, F. Giorgi, and G. T. Bates, A regional climate model for the western United States, *Climatic Change, 15*, 383–422, 1989.

Dickinson, R. E., A. Henderson-Sellers, and P. J. Kennedy, Biosphere-atmosphere transfer scheme (bats) version 1e as coupled to the ncar community climate model, *Tech. rep.*, National Center for Atmospheric Research, 1993.

Emanuel, K. A., A scheme for representing cumulus convection in large-scale models, *J. Atmos. Sci., 48*(21), 2313–2335, 1991.

Emanuel, K. A., and M. Zivkovic-Rothman, Development and evaluation of a convection scheme for use in climate models, *J. Atmos. Sci., 56*, 1766–1782, 1999.

Fairall, C., E. Bradley, J. Godfrey, G. Wick, J. Edson, and G. Young, Cool-skin and warm layer effects on sea surface temperature, *Journal of Geophysical Research, 101*, 1295–1308, 1996.

Fritsch, J. M., and C. F. Chappell, Numerical prediction of convectively driven mesoscale pressure systems. part i: Convective parameterization, *J. Atmos. Sci., 37*, 1722–1733, 1980.

Galperin, B., L. H. Kantha, S. Hassid, and A. Rosati, A quasi-equilibrium turbulent energy model for geophysical flows, *Journal of the Atmospheric Sciences, 45*(1), 55–62, 1988.

Giorgi, F., Two-dimensional simulations of possible mesoscale effects of nuclear war fires, *J. Geophys. Res.*, *94*, 1127–1144, 1989.

Giorgi, F., Simulation of regional climate using a limited area model nested in a general circulation model, *J. Climate*, *3*, 941–963, 1990.

Giorgi, F., and G. T. Bates, The climatological skill of a regional model over complex terrain, *Mon. Wea. Rev.*, *117*, 2325–2347, 1989.

Giorgi, F., and M. R. Marinucci, Validation of a regional atmospheric model over europe: Sensitivity of wintertime and summertime simulations to selected physics parameterizations and lower boundary conditions, *Quart. J. Roy. Meteor. Soc.*, *117*, 1171–1206, 1991.

Giorgi, F., and L. O. Mearns, Introduction to special section: Regional climate modeling revisited, *J. Geophys. Res.*, *104*, 6335–6352, 1999.

Giorgi, F., G. T. Bates, and S. J. Nieman, The multi-year surface climatology of a regional atmospheric model over the western united states, *J. Climate*, *6*, 75–95, 1993a.

Giorgi, F., M. R. Marinucci, and G. T. Bates, Development of a second generation regional climate model (regcm2) i: Boundary layer and radiative transfer processes, *Mon. Wea. Rev.*, *121*, 2794–2813, 1993b.

Giorgi, F., M. R. Marinucci, G. T. Bates, and G. DeCanio, Development of a second generation regional climate model (regcm2) ii: Convective processes and assimilation of lateral boundary conditions, *Mon. Wea. Rev.*, *121*, 2814–2832, 1993c.

Giorgi, F., X. Q. Bi, and Y. Qian, Radiative forcing and regional climatic effects of anthropogenic aerosols over East Asia: A regional coupled climate-chemistry/aerosols model study, *J. Geophys. Res.*, *107*, 2002.

Giorgi, F., X. Q. Bi, and Y. Qian, Indirect vs. direct effects of anthropogenic sulfate on the climate of east asia as simulated with a regional coupled climate-chemistry/aerosol model, *Climatic Change*, *58*, 345–376, 2003a.

Giorgi, F., R. Francisco, and J. S. Pal, Effects of a subgrid-scale topography and land use scheme on the simulation of surface climate and hydrology. part 1: Effects of temperature and water vapor disaggregation., *Journal of Hydrometeorology*, *4*, 317–333, 2003b.

Giorgi, F., J. S. Pal, X. Bi, L. Sloan, N. Elguindi, and F. Solmon, Introduction to the tac special issue: The regcnet network., *Theoretical and Applied Climatology*, *86*, 1–4, 2006.

Grell, G., Prognostic evaluation of assumptions used by cumulus parameterizations, *Mon. Wea. Rev.*, *121*, 764–787, 1993.

Grell, G. A., J. Dudhia, and D. R. Stauffer, Description of the fifth generation Penn State/NCAR Mesoscale Model (MM5), *Tech. Rep. TN-398+STR*, NCAR, Boulder, Colorado, pp. 121, 1994.

Grenier, H., and C. S. Bretherton, A moist pbl parameterization for large-scale models and its application to subtropical cloud-topped marine boundary layers, *Monthly Weather Review*, *129*, 357–377, 2001.

Güttler, I., C. Brankovic, T. A. O'Brien, E. Coppola, B. Grisogono, and F. Giorgi, Sensitivity of regional climate model RegCM4 to planetary boundary layer scheme, 2013.

Hack, J. J., B. A. Boville, B. P. Briegleb, J. T. Kiehl, P. J. Rasch, and D. L. Williamson, Description of the ncar community climate model (ccm2), *Tech. Rep. NCAR/TN-382+STR*, National Center for Atmospheric Research, 1993.

Henderson-Sellers, B., Calculating the surface energy balance for lake and reservoir modeling: A review, *Rev. Geophys.*, *24*(3), 625–649, 1986.

Holtslag, A. A. M., and B. A. Boville, Local versus nonlocal boundary-layer diffusion in a global climate model, *J. Climate*, *6*, 1993.

Holtslag, A. A. M., E. I. F. de Bruijn, and H.-L. Pan, A high resolution air mass transformation model for short-range weather forecasting, *Mon. Wea. Rev.*, *118*, 1561–1575, 1990.

Hostetler, S. W., G. T. Bates, and F. Giorgi, Interactive nesting of a lake thermal model within a regional climate model for climate change studies, *Geophysical Research*, *98*, 5045–5057, 1993.

Hsie, E. Y., R. A. Anthes, and D. Keyser, Numerical simulation of frontogenisis in a moist atmosphere, *J. Atmos. Sci.*, *41*, 2581–2594, 1984.

Kiehl, J. T., J. J. Hack, G. B. Bonan, B. A. Boville, B. P. Breigleb, D. Williamson, and P. Rasch, Description of the ncar community climate model (ccm3), *Tech. Rep. NCAR/TN-420+STR*, National Center for Atmospheric Research, 1996.

Kueppers, L., et al., Seasonal temperature response to land-use change in the western united states., *Global and Planetary Change*, *60*, 2008.

Laurent, B., B. Marticorena, G. Bergametti, J. Leon, and N. Mahowald, Modeling mineral dust emissions from the sahara desert using new surface properties and soil database, *Journal of Geophysical Research*, *113*, d14218, 2008.

Lawrence, P., and T. Chase, Representing a new MODIS consistent land surface in the Community Land Model (CLM3.0), *J. Geophys. Res.*, *112*, g01023, 2007.

O'Brien, T. A., P. Y. Chuang, L. C. Sloan, I. C. Faloona, and D. L. Rossiter, Coupling a new turbulence parametrization to regcm adds realistic stratocumulus clouds, *Geoscientific Model Development*, *5*(4), 989–1008, doi:10.5194/gmd-5-989-2012, 2012.

Oleson, K. e. a., Technical description of the Community Land Model (CLM), *Tech. Rep. Technical Note NCAR/TN-461+STR*, NCAR, 2004.

Oleson, K. W., et al., Improvements to the Community Land Model and their impact on the hydrological cycle, *Journal of Geophysical Research-Biogeosciences*, *113*(G1), 2008.

OBrien, T. A., L. C. Sloan, P. Y. Chuang, I. C. Faloona, and J. A. Johnstone, Multidecadal simulation of coastal fog with a regional climate model, *Climate Dynamics*, pp. 1–12, doi:10.1007/s00382-012-1486-x, 2012.

Pal, J. S., E. E. Small, and E. A. B. Eltahir, Simulation of regional-scale water and energy budgets: Representation of subgrid cloud and precipitation processes within RegCM, *J. Geophys. Res.-Atmospheres*, *105*(D24), 29,579–29,594, 2000.

Pal, J. S., F. Giorgi, X. Bi, et al., The ICTP RegCM3 and RegCNET: Regional climate modeling for the developing world, *Bull. Amer. Meteor. Soc.*, *88*, 1395–1409, 2007.

Patterson, J. C., and P. F. Hamblin, Thermal simulation of a lake with winter ice cover, *Limn. Oceanography*, *33*, 323–338, 1988.

Slingo, J. M., A gcm parameterization for the shortwave radiative properties of water clouds, *J. Atmos. Sci.*, *46*, 1419–1427, 1989.

Small, E. E., and L. C. Sloan, Simulating the water balance of the aral sea with a coupled regional climate-lake model, *J. Geophys. Res.*, *104*, 6583–6602, 1999.

Solmon, F., M. Mallet, N. Elguindi, F. Giorgi, A. Zakey, , and A. Konare, Dust aerosol impact on regional precipitation over western africa, mechanisms and sensitivity to absorption properties, *Geophysical Research Letters*, *35*, l24705, 2008.

Steiner, A. L., J. S. Pal, S. A. Rauscher, J. L. Bell, N. S. Diffenbaugh, A. Boone, L. C. Sloan, and F. Giorgi, Land surface coupling in regional climate simulations of the West African monsoon, *Climate Dynamics*, *33*(6), 869–892, 2009.

Sundqvist, H., E. Berge, and J. E. Kristjansson, The effects of domain choice on summer precipitation simulation and sensitivity in a regional climate model, *J. Climate*, *11*, 2698–2712, 1989.

Tiedtke, M., A comprehensive mass flux scheme for cumulus parameterization on large scale models, *Mon. Wea. Rev.*, *117*, 1779–1800, 1989.

Zeng, X., A prognostic scheme of sea surface skin temperature for modeling and data assimilation, *Geophysical Research Letters*, *32*, l14605, 2005.

Zeng, X., M. Zhao, and R. E. Dickinson, Intercomparison of bulk aerodynamic algoriths for the computation of sea surface fluxes using toga coare and tao data, *J. Climate*, *11*, 2628–2644, 1998.

**BATS** Biosphere-Atmosphere Transfer Scheme

**BATS1e** Biosphere-Atmosphere Transfer Scheme version 1e

**CAM** Community Atmosphere Model

**CAPE** convective available potential energy

**CCM** Community Climate Model

**CCM1** Community Climate Model version 1

**CCM2** Community Climate Model version 2

**CCM3** Community Climate Model version 3

**CLM** Community Land Surface Model

**CLM0** Common Land Model version 0

**CLM2** Community Land Model version 2

**CLM3** Community Land Model version 3

**CMAP** CPC Merged Analysis of Precipitation

**CRU** Climate Research Unit

**CPC** Climate Prediction Center

**ECMWF** European Centre for Medium-Range Weather Forecasts

**ERA40** ECMWF 40-year Reanalysis

**ESMF** Earth System Modeling Framework

**ESP** Earth Systems Physics

**FAO** Food and Agriculture Organization of the United Nations

**fvGCM** NASA Data Assimilation Office atmospheric finite-volume general circulation model

**GLCC** Global Land Cover Characterization

**GCM** General Circulation Model

**HadAM3H** Hadley Centre Atmospheric Model version 3H

**ICTP** Abdus Salam International Centre for Theoretical Physics

**IPCC** Intergovernmental Panel on Climate Change

**IBIS** Integrated BIosphere Simulator

**LAI** leaf area index

**LAMs** limited area models

**LBCs** lateral boundary conditions

**MC2** Mesoscale Compressible Community model

**MIT** Massachusetts Institute of Technology

**MM4** Mesoscale Model version 4

**MM5** Mesoscale Model version 5

**MERCURE** Modelling European Regional Climate Understanding and Reducing Errors

**NNRP** NCEP/NCAR Reanalysis Product

**NNRP1** NCEP/NCAR Reanalysis Product version 1

**NNRP2** NCEP/NCAR Reanalysis Product version 2

**NCAR** National Center for Atmospheric Research

**NCEP** National Centers for Environmental Prediction

**PBL** planetary boundary layer

**PC** Personal Computer

**PIRCS** Project to Intercompare Regional Climate Simulations

**PFT** plant functional type

**PSU** Pennsylvania State University

**PWC** Physics of Weather and Climate

**RCM** Regional Climate Model

**RegCM** REGional Climate Model

**RegCM1** REGional Climate Model version 1

**RegCM2** REGional Climate Model version 2

**RegCM2.5** REGional Climate Model version 2.5

**RegCM3** REGional Climate Model version 3

**RegCM4** REGional Climate Model version 4

**RegCNET** REGional Climate Research NETwork

**RMIP** Regional Climate Model Intercomparison Project

**ROMS** Regional Oceanic Modeling System

**SIMEX** the Simple EXplicit moisture scheme

**SST** sea surface temperature

**SUBEX** the SUB-grid EXplicit moisture scheme

**USGS** United States Geological Survey

**JJA** June, July, and August

**JJAS** June, July, August, and September

**JFM** January, February, and March